ACS APPLIED MATERIALS & INTERFACES

Research Article

www.acsami.org

Water-Responsive Mechanically Adaptive Nanocomposites Based on Styrene–Butadiene Rubber and Cellulose Nanocrystals—Processing Matters

Pratheep K. Annamalai,[†,§,⊥] Koffi L. Dagnon,[‡,§] Seyedali Monemian,[‡] E. Johan Foster,[†] Stuart J. Rowan,*[,‡] and Christoph Weder*[,†]

[†]Adolphe Merkle Institute, University of Fribourg, Route de l'Ancienne Papeterie, 1723 Marly, Switzerland

[‡]Department of Macromolecular Science and Engineering, Case Western Reserve University, 2100 Adelbert Road, Cleveland, Ohio 44106-7202, United States

Supporting Information

ABSTRACT: Biomimetic, stimuli-responsive polymer nanocomposites based on a hydrophobic styrene–butadiene rubber (SBR) matrix and rigid, rod-like cellulose nanocrystals (CNCs) isolated from cotton were prepared by three different approaches, and their properties were studied and related to the composition, processing history, and exposure to water as a stimulus. The first processing approach involved mixing an aqueous SBR latex with aqueous CNC dispersions, and films were subsequently formed by solution-casting. The second method utilized the first protocol, but films were additionally compression-molded. The third method involved the formation of a CNC organogel via a solvent exchange with acetone, followed by infusing this gel, in which the CNCs form a percolating network with solutions of SBR in tetrahydrofuran. The thermomechanical properties of the materials were established by dynamic mechanical thermal analysis (DMTA). In the dry state, all nanocomposites show much higher tensile storage moduli, E', than the neat SBR or the SBR latex. E' increases with the CNC content and depends strongly on the processing method, which appears to influence the morphology of the SBR nanocomposites produced. The highest E' values were observed for the solution cast samples involving an SBR latex, where E' increased from 3 MPa for the neat SBR to ca. 740 MPa for the nanocomposite containing 20% v/v CNCs. Upon submersion in deionized water, a dramatic reduction of E' was observed, for example from 740 to 5 MPa for the solution-cast nanocomposite containing 20% v/v CNCs. This change is interpreted as a disengagement of the percolating CNC network, on account of modest aqueous swelling and competitive hydrogen bonding of water molecules with the CNCs. It is shown that the method of preparation also influenced the swelling behavior and kinetics of modulus switching, consistent with different arrangements of the CNCs, which serve as channels for water absorption and transport within the hydrophobic SBR matrix.

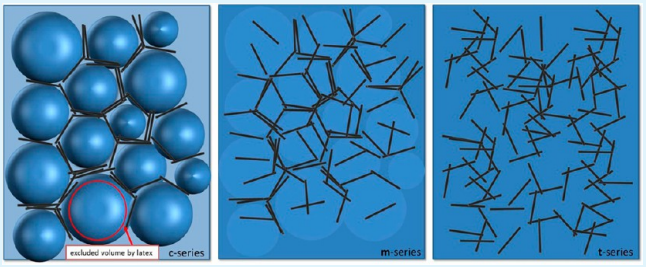

KEYWORDS: *nanocomposites, styrene–butadiene rubber, cellulose nanocrystals, water-responsive behavior, processing, stimuli-responsive, mechanically adaptive*

INTRODUCTION

Stimuli-responsive, polymeric materials that respond to external stimuli, such as exposure to light, heat, chemicals, magnetic fields, etc., with a change of at least one of their properties have gained significant attention from researchers in both academia and industry.[1] Motivated by the objective to create mechanically adaptive, stimuli-responsive materials, which are rigid in their original state, but soften upon command, we developed a new approach to chemically responsive, mechanically adaptive polymer nanocomposites.[2−4] These materials mimic the architecture and function of the skin of sea cucumbers, which can change its stiffness when needed. Our artificial nanocomposites are comprised of low-modulus polymer matrices and rigid cellulose nanofibers, also referred to as "cellulose whiskers" or "cellulose nanocrystals" (CNCs).[5−8] The interactions between the CNCs, which form percolating networks within the polymer matrix and perhaps also between the CNCs and the polymer matrix, can be mediated by exposing the nanocomposite to water.[9−11] Upon modest aqueous swelling, the reinforcing CNC network is disrupted due to competitive hydrogen bonding of the CNCs to water, resulting in a dramatic modulus reduction.[12] Much of our previous work has focused on the design of materials that change their mechanical properties upon exposure to physiological conditions[4,13,14] and are useful for adaptive medical implants.[15−18] The approach has also been extended to shape-memory materials,[19] pH-responsive nanocomposites,[20] light-responsive healable nanocomposites,[21] and water-

Received: October 6, 2013
Accepted: December 19, 2013
Published: December 20, 2013

responsive nanocomposites based on hydrophobic matrices.[22] The latter were based on CNCs isolated from tunicates and poly(styrene-*co*-butadiene) or poly(butadiene) as the matrix. While the CNCs and these hydrophobic polymers are *a priori* not miscible, their nanocomposites can be accessed by a template approach,[23] in which CNC organogels are first created via a sol−gel method. These gels are composed of percolating networks of CNCs willed with solvent and can be infused with solutions of SBR to afford nanocomposites in which CNCs are well-dispersed. (As an alternative approach for processing CNCs with hydrophobic polymers on an industrial scale, lyophilizate from miscible polymer−CNCs dispersion can also be accessed[24]). Despite the hydrophobic nature of the matrix polymers, these nanocomposites displayed pronounced water-induced stiffness changes. The level of reinforcement, the amount of water uptake, and the kinetics of the switching process depended strongly on the CNC content, suggesting that the highly polar CNCs serve as hydrophilic channels[25] that promote water transport into the hydrophobic matrix.[22]

Using SBR as the matrix and CNCs isolated from cotton, which have a lower aspect ratio (ca. 10) than the tunicate-based CNCs used in our previous study but are more accessible, we discuss here in how processing influences the stimuli-responsive properties of nanocomposites comprised of a hydrophobic matrix and a hydrophilic filler. Nanocomposites were made by three different processes and their properties were studied and related to the composition, processing history, and exposure to water as a stimulus. The first approach followed the protocol first utilized by Favier et al.[26] and involved the production of films by mixing an aqueous SBR latex with aqueous CNC dispersions, solution-casting and subsequent drying. The next method utilized this same protocol, but the films were additionally reshaped by compression molding. The final protocol utilizes an approach we had previously employed to access the SBR tunicate CNC nanocomposites,[22] namely the formation of a CNC organogel template that was infused with solutions of SBR followed by drying and compression-molding. Our systematic investigation of the mechanical properties of these materials in the dry and wet state shows a significant influence of the processing history, consistent with different arrangements of the CNCs within the hydrophobic SBR matrix.

EXPERIMENTAL SECTION

Materials. The styrene−butadiene rubber (SBR) was supplied as a solid (23.5% bound styrene, M_w = 215 000 g/mol, PDI = 1.8, density = 0.94 g/cm^3) and as latex (SBR-1502, weight-average molecular weight, M_w = 179 000 g/mol, polydispersity index, PDI = 2.12, latex pH = 9.9, solid content = 22.6%, dry weight = 0.914 g/mL, average particle diameter as measured by light scattering = 60 nm). All solvents were purchased from Fisher Scientific (Pittsburgh, PA) and were used as received, except acetone, which was dried over anhydrous potassium carbonate. Cellulose nanocrystals (CNCs) were isolated from Whatman no. 1 filter paper via sulfuric acid hydrolysis using the previously reported procedure (see the Supporting Information).[23,27] Multiple batches of CNCs obtained via this protocol were used for preparing nanocomposites. Their microscopic and conductometric measurements showed similar results. After the hydrolysis, their average diameter and length were found to be 365 ± 80 × 34.5 ± 6.1 nm from the analysis of transmission electron microscopic (TEM) images using Image-J (Java-based online image processing program developed by the National Institutes of Health, Bethesda, MD). At least 50 CNCs were measured for each sample. The concentration of negatively charged sulfate groups on the surface of the CNCs was determined by conductometric titration of aqueous suspension of freeze-dried CNCs (75 mL of a dispersion with a CNC concentration of 1 mg/mL were titrated against 0.01 M of aqueous KOH) to be 35 ± 2 mmol/kg. A density of 1.42 g/cm^3 was used for the CNCs for further calculations, assuming a crystallinity of approximately 70−88%, as was previously reported.[28−30] For preparing nanocomposites via solution casting, the aqueous CNC suspension was directly used; whereas for the template approach, the suspension was further freeze-dried and redispersed in water before the CNC organogel template was formed (see the Supporting Information).

Fabrication of SBR/CNC Nanocomposites via Solution Casting and Compression-Molding. Aqueous suspensions of CNCs (20 mg/mL) obtained from hydrolysis were stirred for 3 h and ultrasonicated for 1 h in an ultrasonic bath (USC600TH of VWR) which operates at 45 kHz. Premeasured quantities of the CNC suspension were subsequently added to the SBR latex, and the CNC/SBR mixtures were stirred for 3 h and ultrasonicated for 1 h. For example, to obtain a SBR/CNC nanocomposite with 9% v/v CNCs, 19 mL of the CNC dispersion were combined with 13 mL of the SBR latex. Volume fractions of CNCs were calculated using a solid content and density of latex of 22.6 wt % and 0.914 g/mL, respectively (i.e., 2.63 g of solid content SBR in 13 mL of latex), density of the neat SBR matrix 0.94 g/cm^3, and density of CNCs 1.42 g/cm^3. The resulting mixtures were cast into Teflon Petri-dishes, and the solvent was evaporated at 40 °C in a ventilated oven for 2−3 days, resulting in nanocomposite films of a thickness of 510 ± 110 μm.

Portions of the films thus made were further compression-molded at 3000 psi in a Carver Press between Teflon sheets at 120 °C for 15 min, using spacers to control the thickness, and subsequently cooled to room temperature to yield 480 ± 110 μm thick films. Pressing conditions were optimized to obtain nonshrinking, free-standing films. Control samples of neat SBR were also prepared using the above-described casting and compression-molding methods. The sample codes for solution cast and compression-molded nanocomposite films are "**xc**" and "**xm**", respectively, where "**x**" represents the loading of CNCs (% v/v).

Fabrication of SBR/CNC Nanocomposites via the Template Approach. A template approach similar to the one previously reported by Capadona et al.[2,23,31] was also used to fabricate SBR/CNC nanocomposites. In a typical experiment, an aqueous CNCs dispersion (50 mL with a CNC concentration of 12 mg/mL) was prepared by ultrasonicating the freeze-dried CNCs for 48 h and finally degassed by heating at 80 °C for 10 min and shaking manually. After cooling to room temperature, acetone (50 mL) was gently added along the wall of the beaker, to avoid mixing with the aqueous CNC dispersion, to form an organic layer on top of the aqueous dispersion. Acetone gradually diffuses into the water and the top layer was exchanged with fresh acetone daily until the bottom portion had assembled into a mechanically coherent CNC/acetone gel (typically 8−10 days). The acetone layer was gently agitated from time to time to facilitate the solvent exchange. Eventually, the acetone gel was released from the beaker, and washed with dry acetone. The resulting gel was cut into rectangular pieces (1 cm × 0.75 cm × 1.5 cm), which were stored in dry acetone until used. Gravimetric analysis showed the CNC content in the acetone gels to be 1.5%w/w, which represents the ratio of dry (at 40 °C for 24 h) and wet weight of organogel.

Solid SBR was dissolved in anhydrous tetrahydrofuran (THF) at concentrations ranging from 30 to 125 mg/mL by stirring overnight at room temperature. Pieces of the CNC organogel, prepared as described above, were weighed and placed at room temperature into these SBR solutions for 16 h. The gels were subsequently removed from the polymer solutions and dried at ambient temperature in a well-ventilated fume hood for 6 h to remove the majority of the solvent. They were subsequently placed in a vacuum oven at 50 °C for another 24 h to remove any residual solvent. The dried materials were compression-molded in a Carver Press between Teflon sheets at 3000 psi pressure at room temperature for 2 min and 75 °C for 10 min to yield 500 ± 50 μm thick SBR nanocomposite films, which were allowed to cool to room temperature. Pressing conditions were optimized to obtain nonshrinking, free-standing films. A control sample of the neat SBR was prepared using the same procedure. The CNC volume fraction in the final nanocomposites was calculated

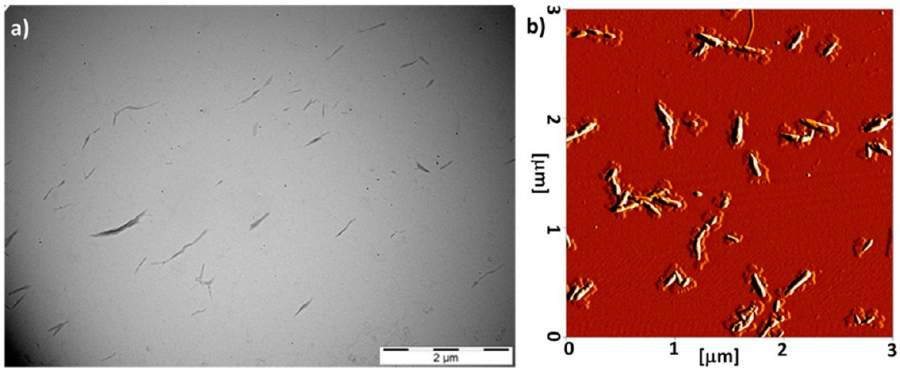

Figure 1. (a) Transmission electron micrograph of the CNCs obtained via acid hydrolysis. Concentration of CNCs suspension 0.08 mg/mL; average dimensions = 365 ± 80 nm × 34.5 ± 6.1 nm. (b) Atomic force micrograph (height image) of CNCs. Concentration of CNC suspension = 0.008 mg/mL.

based on the weight fraction of the CNCs in the polymer, using a density of 1.42 g/cm^3 for the CNCs and a density of 0.94 g/cm^3 for SBR. The weight fraction was determined gravimetrically from the weight (in milligrams) of CNCs in the wet CNC organogels used to prepare the nanocomposites (this weight was determined by drying the organogel at 40 °C for 24 h) and the weight of the final nanocomposite. These "template-made" nanocomposite films are coded as "**xt**" where **x** represents the loading of CNCs (% v/v).

Microscopic Analyses of CNCs and SBR/CNC Nanocomposites. Samples for TEM analyses were prepared by depositing a 10 μL drop of a 0.08 mg/mL aqueous CNC suspension onto a copper grid supported by a 3 nm carbon layer with a 50 nm layer polymer film below. The samples were dried at 60 °C in a vacuum oven for 2 h, and images were taken using a Philips Electron Optics CM100 TEM operating at an accelerating voltage of 80 kV. SBR/CNCs nanocomposite films (**17c** and **14t**) were cryo-microtomed at −70 °C using a Leica Ultramicrotome UC6 equipped with a Diatome cryodiamond knife. Images of microtomed specimen were recorded without any prior staining using a JEOL 1200EX TEM operating at 80 kV. Samples for atomic force microscopic (AFM) analyses were prepared by depositing a 10 μL drop of a 0.008 mg/mL aqueous CNC dispersion onto a freshly cleaved mica surface and drying at 60 °C in a vacuum oven for 30−45 min. A NanoWizard II (JPK Instrument, Germany) was used to acquire images using tapping mode in air with a scan rate of 1 line/s. To examine the morphology of SBR/CNC nanocomposites, thin films were mounted on clean glass microscopy slides and samples were scanned using the same experimental conditions. The CNC dimensions were determined by analyzing 5 TEM images individually for both type of CNCs and measuring length and width of at least 50 CNCs.

Dynamic Mechanical Thermal Analysis (DMTA). The thermomechanical properties of the neat SBR samples and the SBR/CNC nanocomposites were measured with a dynamic mechanical analyzer Model Q800 (TA Instruments, New Castle, USA), operating in the tensile mode. Prior to the measurement, the samples were dried in a ventilated oven in the case of the solution-cast (**c**) and solution-cast/compression-molded (**m**) samples, and in a vacuum oven for the samples made by the template process (**t**). Tensile moduli of the samples in the dry state were established by temperature sweeps from −100 to 100 °C with a scanning rate of 5 °C/min for **c** and **m** samples and 3 °C/min for **t** samples. In order to determine the tensile moduli of the samples in the water-swollen state and the kinetics of the water-induced stiff-soft transition, DMTA experiments were also conducted using submersion clamps, which allowed measurements while the samples were immersed in water. In this case, samples were tested isothermally at 37 °C for the **c** and **m**-series, and at 25 °C for the **t**-series. Reference experiments show that the slightly different heating rate and swelling temperature do not measurably impact the data.

To measure stiffness during drying and wetting, the instrument was stopped to allow removal or addition of water, using a pipet. The furnace was subsequently closed and the scanning resumed, isothermally. The interrupted time (2−3 min) was also included/normalized in the plotted graph.

Aqueous Swelling Behavior. The aqueous swelling behavior of nanocomposite films was monitored in deionized water at 37 °C for **c** and **m** series and at 25 °C for the **t** series. The specimen in the form of rectangular films were first dried for 24 h under vacuum at 60 °C and weighed using a microbalance. They were subsequently immersed in deionized water, removed every 24 h, gently blotted using filter paper, weighed, and immediately reimmersed in deionized water. Swelling measurements were done in triplicate and conducted over a period of 6 days (for the **c** and **m** series) and 10 days for the **t**-series nanocomposites. For the latex-based systems (**c** and **m**), swelling for longer than 6 days resulted in degradation of the film and the observation of colloidal particles in the water. The water uptake, expressed as swelling degree (%), was determined from the relative weight gain of the samples by

$$\text{swelling degree}(\%) = \frac{M_t - M_0}{M_0} \times 100 \quad (1)$$

where M_0 and M_t are the mass of the sample before and after exposure to deionized water for time t, respectively.

The mean water uptake was further calculated for various exposure times for **t**-series. The mass of water absorbed at time t ($M_t - M_0$) can be expressed as[32]

$$\frac{M_t - M_0}{M_\infty} = 1 - \sum_{n=0}^{n=\infty} \frac{8}{(2n+1)^2\pi^2} \exp\left[\frac{-D(2n+1)^2\pi^2 t}{(2L)^2}\right] \quad (2)$$

where M_∞ is the mass of the sample after equilibrium swelling, $2L$ is the initial thickness of the film, and D the diffusion coefficient. Equation 2 represents a Fickian mode of diffusion. After the equilibrium swelling, a slight change in thickness of the nanocomposite films was observed and this change was dependent on the CNC content. For short immersion period, i.e. at low $(M_t - M_0)/M_\infty$ values (<0.5), eq 2 can be rewritten as[22,32]

$$\frac{M_t - M_0}{M_\infty} = \frac{2}{L}\left(\frac{D}{\pi}\right)^{1/2} t^{1/2} \quad (3)$$

RESULTS AND DISCUSSION

Isolation and Properties of CNCs. The CNCs used in this study were isolated from Whatman filter paper by sulfuric acid following the previously reported procedure.[23,27] The concentration of negatively charged sulfate groups on the surface of the CNCs, which are introduced during hydrolysis and influence the dispersibility, thermal stability,[28] and hydrophilicity of the CNCs, was determined by conductometric titration to be 35 ± 2 mmol/kg. This number is important to

note as the charge density on the CNCs has been shown to impact the degree of swelling and rate of the water-induced mechanical switching.[33] Figure 1 shows TEM and atomic force microscopic (AFM) micrographs of the CNCs, which reveal that before processing into nanocomposites the CNCs were well individualized and display the characteristic nanorod-like features, with an average length of 365 ± 80 nm and an average diameter of 34.5 ± 6.1 nm (determined from TEM images). From these values an aspect ratio of 10.5 ± 0.4 was calculated.

Preparation of SBR/CNC Nanocomposite Films by Solution Casting and Compression-Molding. Nanocomposite films based on a SBR latex and 1−20% v/v CNCs were first made by combining the required amount of an aqueous CNC dispersion with the latex, ultrasonicating the mixture, and casting the resulting mixtures into a mold (see the Experimental Section for details). The solvent was slowly evaporated at a temperature of 40 °C, resulting in smooth transparent nanocomposite films of a thickness of ca. 510 ± 110 μm (**c**-series). It is worthwhile noting that the temperature at which the solvent is evaporated was important; nanocomposite films dried at higher temperature (e.g., at 50 °C) developed cracks, while films dried at a temperature below minimum film formation temperature, e.g. at 35 °C, were hazy. Portions of the films thus made were further compression-molded at 120 °C to yield 480 ± 110 μm thick films (**m**-series). After molding using 250 μm thicker spacers, slight shrinkage in the plane of the films was observed upon removing the films from the Teflon sheets between which they were pressed, accompanied with a slight increase in thickness due to the elasticity of the SBR. This shrinkage was controlled with increasing content of CNCs, presumably due to increased network formation.

Preparation of SBR/CNC Nanocomposite Films via Template Approach Followed by Compression-Molding. A template approach following the procedure previously reported was used to fabricate nonlatex SBR/CNC nanocomposite films.[2,23,31] In brief, acetone was placed on top of an aqueous CNC dispersion (see the Experimental Section and Supporting Information for details) such that the organic solvent gradually replaced the water and the bottom portion eventually assembled into a mechanically coherent CNC/acetone gel. The CNC organogel was placed into solutions of SBR in anhydrous tetrahydrofuran. The composition of the nanocomposites was controlled via the concentration of the SBR solution. Solutions with a SBR concentration of >125 mg/mL which would be required to produce nanocomposites with a CNC content of <10% v/v have a high viscosity that prevents efficient filling of the template. The SBR/CNC/tetrahydrofuran gels were subsequently dried and the materials were compression-molded to yield 500 ± 50 μm thick films (**t**-series) with a CNC content of 10−22% v/v. The processing temperature was varied over a broad range to establish a regime where extensive shrinking in the lateral dimension due to the rubber elasticity of the SBR (pronounced if processed at low temperature[22]), and thermal degradation of the CNCs (pronounced at temperatures above 150 °C[34,35]). The best conditions which afforded films that showed minimal shrinkage, involved first pressing the nanocomposites at room temperature and subsequently increasing the temperature to 75 °C. It is also worthwhile noting that the shrinking of the film during compression-molding decreases substantially with increasing the volume fraction of CNCs.

Mechanical Properties of the SBR/CNC Nanocomposites. To investigate the effect of the CNCs on the thermomechanical properties in the linear viscoelastic regime, neat SBR and SBR/CNC nanocomposite films made by the solution casting, solution casting plus compression-molding, and the template approach were probed by dynamic mechanical thermal analysis (DMTA). Figure 2 shows the tensile storage

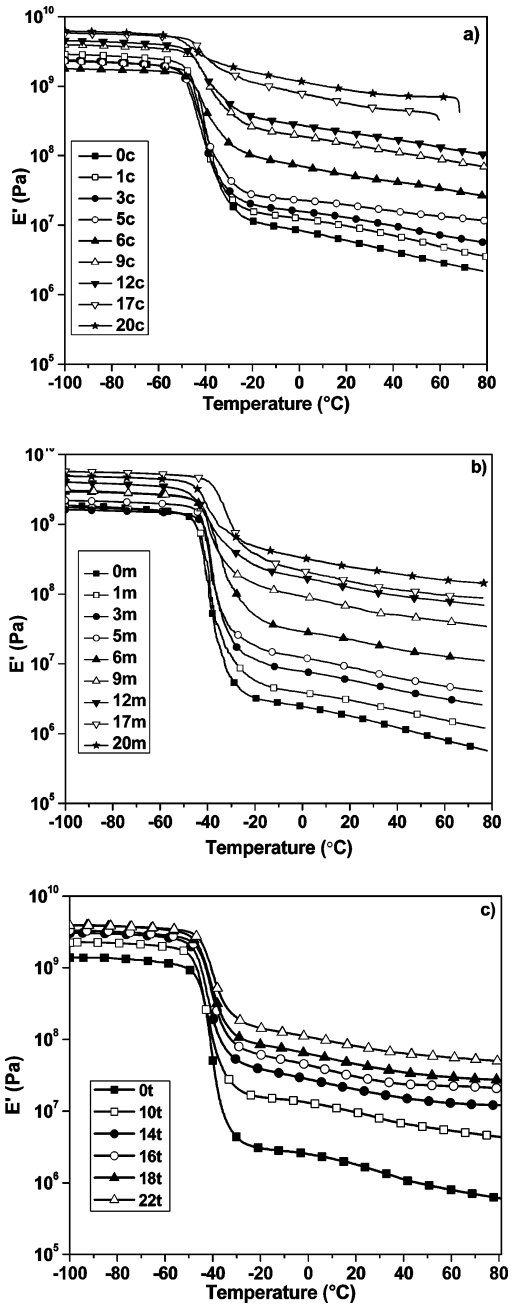

Figure 2. Dynamic mechanical thermal analysis traces of dry films of SBR and SBR/CNC nanocomposites. (a−c) Tensile storage modulus E' as a function of CNC content and temperature for solution cast (**c**), compression-molded (**m**), and template-made (**t**) samples.

modulus E' (a−c) versus temperature for all samples, and the loss tangents are shown in Figure S1 in the Supporting Information. Table 1 summarizes the values of E' in the glassy (−80 °C) and rubbery (25 °C) regimes for all the samples. The E' curves of samples **0c**, **0m**, and **0t** (corresponding to the SBR latex (**0c**, **0m**) or SBR (**0t**) matrices processed by solution casting, casting- and compression-molding, and the template

dx.doi.org/10.1021/am404382x | ACS Appl. Mater. Interfaces 2014, 6, 967−976

Table 1. Tensile Storage Modulus E' (MPa) of Dry Films of Neat SBR and SBR/CNC Nanocomposite Films in the Glassy (−80 °C) and Rubbery (at 25 °C) Regimes[a]

	solution casting (SBR latex)		casting and compression-molding (SBR latex)		template approach SBR		
	glassy state (− 80 °C)	rubbery state (25 °C)	glassy state (−80 °C)	rubbery state (25 °C)		glassy state (−80 °C)	rubbery state (25 °C)
CNC content (% v/v)	E' (MPa)	E' (MPa)	E' (MPa)	E' (MPa)	CNC content (% v/v)	E' (MPa)	E' (MPa)
0	1630 ± 400	3 ± 1	1771 ± 222	2 ± 0.6	0	1339 ± 157	1 ± 0.2
1	2621 ± 71	8 ± 1	1661 ± 169	3 ± 0.7			
3	2198 ± 20	13 ± 1	1789 ± 167	5 ± 0.5			
5	2258 ± 63	27 ± 5	2184 ± 136	8 ± 0.5			
6	2448 ± 72	51 ± 2	2701 ± 93	18 ± 2	10	2200 ± 275	12 ± 2
9	3624 ± 110	136 ± 3	3095 ± 88	46 ± 9	14	2957 ± 105	23 ± 3
12	3410 ± 643	171 ± 36	3729 ± 83	101 ± 25	16	3170 ± 186	34 ± 3
17	5431 ± 133	428 ± 75	5257 ± 193	116 ± 15	18	3771 ± 70	45 ± 4
20	5377 ± 430	736 ± 79	4385 ± 196	210 ± 15	22	3809 ± 15	78 ± 6

[a]Experimental data points determined from DMTA measurements represent averages (number of individual measurement, N = 3−4) ± standard error measurements.

process, respectively) are virtually identical and show the characteristic features of amorphous, high-molecular-weight SBR, i.e. an E' of ca. 1.6 ± 0.4 GPa in the glassy state (−80 °C), a glass transition (T_g) temperature of around −39 °C, and a rubbery plateau, where E' slightly decreases with increasing temperature and is about 3 ± 1 MPa at 25 °C. Inspection of Figure 2a−c shows that reinforcement occurs in all three series and E' increases with the CNC content. As is seen in other matrices and with other CNCs, the increase in E' is much more pronounced in the rubbery regime than in the glassy state.

In the glassy regime, the reinforcement effect is slightly dependent on the processing method. For example, at −80 °C, samples containing 20% v/v CNCs made by solution casting and solution casting plus compression-molding display tensile storage moduli of E' of 5.4 ± 0.4 (**20c**) and 4.4 ± 0.2 GPa (**20m**); whereas the sample containing 22% v/v CNCs made by the template approach (**22t**) displayed an E' of 3.8 ± 0.1 GPa (Table 1). The processing method did have a more pronounced effect on the level of reinforcement observed in the rubbery regime. While in all three series E' increased steadily with the CNC concentration, the reinforcement was most pronounced in the case of the solvent-cast latex-based samples, where E' at 25 °C increased from 3 to 736 MPa for a sample with 20% v/v CNCs (**20c**, Table 1). The compression-molded sample of the same composition, measured under the same conditions, exhibited an E' of only 210 MPa (**20m**, Table 1), and the template-made sample containing 22% v/v CNCs displayed an E' of only 78 MPa (**22t**, Table 1).

The significant increase of the storage modulus in polymer/CNC nanocomposites in the regime above T_g is often attributed to the formation of a percolating network of CNCs. The level of reinforcement of CNC can be described by a percolation model,[18,28,29,32] which assumes that under conditions where the modulus of the matrix polymer (E_m) is much lower than that of the rigid percolating network formed by the filler particles (E_r), the tensile storage modulus E' of the nanocomposite is largely a function of the volume fraction and the modulus E_r of the rigid percolating network. Using a value of 10.5 for the aspect ratio A and the previously reported storage modulus for the rigid phase (E_r) of 0.65 GPa[13,23] in the percolation model (see the Supporting Information), the dry-state data sets (Figure 3a−c) shows that only in the case of the nanocomposites formed via the template approach (**t**-series) the experimental data matches well with the prediction of the percolation model, while the other two materials series (**c**- and **m**-series) show a greater level of reinforcement than predicted by the model.

In addition to the formation of a percolating CNC network in which CNCs interact presumably predominantly via hydgrogen-bonding, interactions between the CNCs and the polymer matrix must also be considered. However, the larger than expected reinforcement of the CNCs in the latex-based nanocomposites appears to suggest that something more complex is going on in these systems than a simple homogenously dispersed CNC network. One possible explanation could be the formation of a different CNC network morphology as represented in Figure 4, which shows a schematic representation of possible morphology differences in samples obtained via casting at 40 °C (**c**-series), compression-molding at 120 °C (**m**-series), and template-approaches at 75 °C (**t**-series).

In the case of the latex based samples (Figure 4 **c**-series, left), the morphology of the films depends on the degree of the "coalescence" which involves compaction, deformation, cohesion, and interdiffusion of polymer chains from the individual latex particles that are typically stabilized by electrostatic and/or steric interactions rendered by adsorbed surfactants or charged end groups of polymers. Upon evaporation of the continuous phase (i.e., water), these interactions or any other forces resisting particle deformation can be overcome for the higher degree of coalescence which depends on casting temperature. As mentioned above, the temperature was optimized to be 40 °C, in order to obtain transparent and smooth nanocomposite films. At this temperature, the complete coalescence, i.e. interdiffusion of nonpolar polymer (SBR) chains, may be affected/limited in presence of charged CNCs (polar). In other words, the initial SBR droplets, which have a diameter of ca. 60 nm, may either retain their particle-structure or may coalesce to form larger particles and as such exclude a large volume into which the CNCs cannot enter. As a result, the CNCs must concentrate in the interstitial space and result in a much better reinforcement, than in the case where the CNCs are well-dispersed (Figure 4 **t**-series, right). This behavior has been reported before by Dubief et al.[36] In the **m**-series, this structure

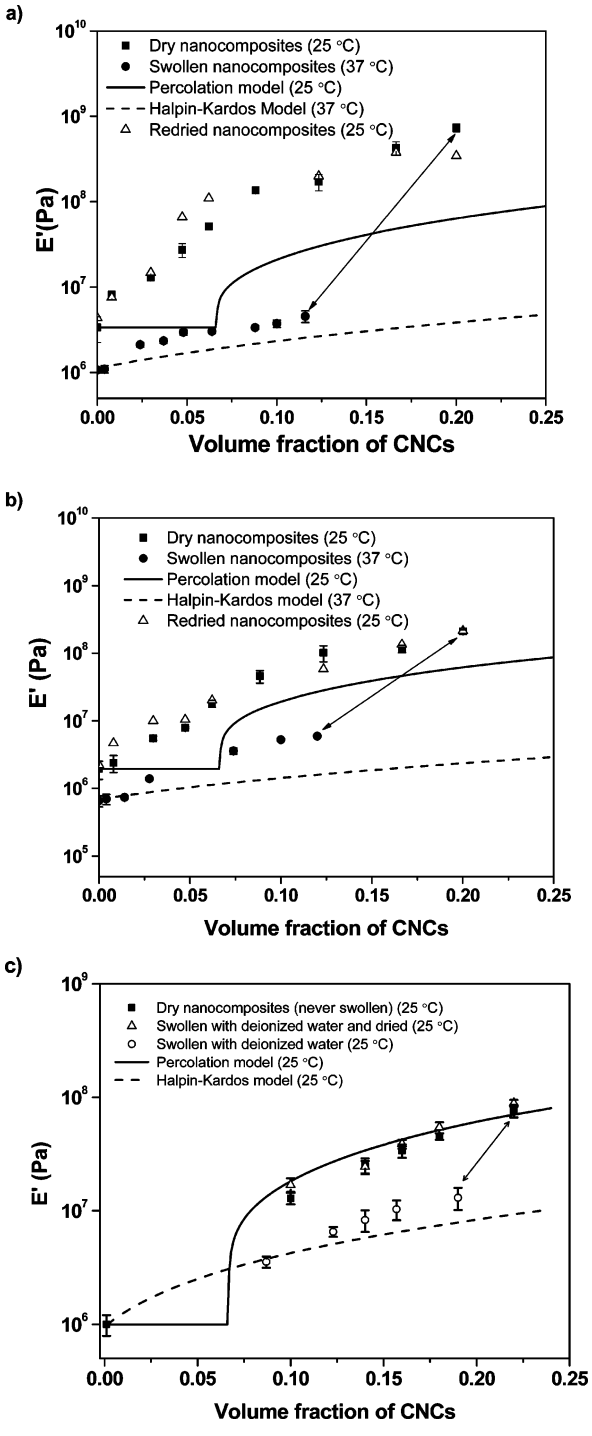

Figure 3. Tensile storage moduli E' of SBR/CNC nanocomposite films at 25 °C made by (a) solution-casting (**c**-series), (b) casting and compression-molding (**m**-series), and (c) the template approach (**t**-series) as a function of volume fraction of CNCs. Filled squares represent the dry-state E', filled circles represent E' in the water-swollen state after equilibrium swelling in deionized water for 5 or 6 days (**c**- and **m**-series) and 10 days (**t**-series), and open triangles represent E' after redrying the water-swollen samples at 60 °C for 48 h. The solid lines show the values predicted by the percolation model for the dry state, whereas dashed lines represent those predicted by the Halpin-Kardos model for the water-swollen wet state. The arrows indicate changes in modulus and volume fraction of CNCs resulting from aqueous swelling of nanocomposites **20c**, **20m**, and **22t**. Experimental data points represent averages (number of individual measurement, N = 3–4) ± standard error measurements.

may be somewhat deteriorated by compression-molding at 120 °C (Figure 4 **m**-series, middle), and as a result these materials display an intermediate level of reinforcement.

To probe the difference in the morphology, the dispersion of CNCs in the **c**-series and **t**-series was further examined by transmission electron microscopy in the nanocomposites with CNC loading above theoretical percolation threshold. Figure 5 shows the TEM images of cryo-microtomed nanocomposites obtained (a) via solution casting with 17% v/v CNCs loading and (b) via template-approach with 14% CNCs loading. Both representative images show individual CNCs and confirm the absence of large-scale phase separation. For the **17c** sample (Figure 5a), in addition to the dispersed CNCs, physically connected/bundled CNCs at the interstitial space can also be viewed, consistent the above-explained morphology.

Aqueous Swelling Behavior of SBR/CNC Nanocomposites. We showed previously for several polymer/CNC nanocomposites that the stiffness is significantly reduced if water diffuses into the nanocomposite and disengages the percolating CNC network by way of competitive hydrogen bonding.[2,4,13,19] Thus, the water uptake capability of the new SBR/CNC nanocomposites in deionized water was investigated, to probe the influence of aqueous swelling on their mechanical properties. Solution-cast and compression-molded nanocomposite films were subjected to swelling at 37 °C for 6 days, whereas the nanocomposite films obtained by the template approach were subjected to swelling at room temperature for 10 days (Figure 6).

It can be observed that both the rate of water uptake and the degree of swelling of these nanocomposites are a function of three parameters, namely the polymer matrix, the CNC content and the processing technique. In general, the rate of water uptake decreases with time (Figure 6a–c). For the latex nanocomposite films (Figure 6a), a plateau corresponding to equilibrium swelling was reached in about 5 days for samples with a CNCs content of 6% v/v or higher, while samples with a CNC content of less than 6% v/v do not reach the equilibrium state by that time. The equilibrium degree of swelling of the solution-cast samples *decreased* from 56% for the latex based SBR (**0c** sample) to 44% for the 20% v/v CNC nanocomposites (**20c**) (Figure 6d). The high water uptake of the neat SBR (**0c**) is at a first glance surprising, but it is consistent with the presence of hydrophilic surfactants present in the latex through which water can be absorbed and form channels through the films.[37,38] With the incorporation of CNCs, whose surface functional groups can interact well with the surfactants of latex particles, the mechanical integrity of the films gradually increases, and this appears to slightly reduce the equilibrium swelling degree. The introduction of CNCs does, however, decrease the time after which the equilibrium has been reached, consistent with the hydrophilic nature of the CNCs (vide infra).

The compression-molded nanocomposite films show, by and large, a very similar behavior (Figure 6b) as the solution-cast samples, indicative of the fact that for the latex-based materials, the water uptake is mainly dictated by the composition and not the processing method.

The nanocomposite films made by the template approach (Figure 6c), show a rather different swelling behavior. Here, the neat SBR shows a much smaller equilibrium water uptake (6%) than the latex-based SBR, consistent with the absence of (or much smaller concentration) of surfactant in the SBR used to create the template-made samples. In the **t**-series, the

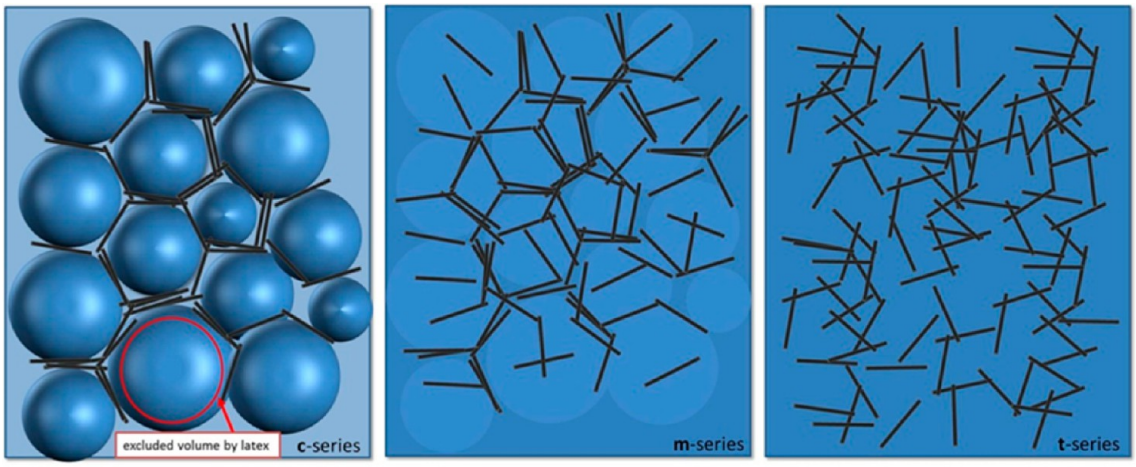

Figure 4. Schematic representation of possible morphology differences in samples obtained via casting at 40 °C (**c**-series), compression-molding at 120 °C (**m**-series), and template-approaches at 75 °C (**t**-series).

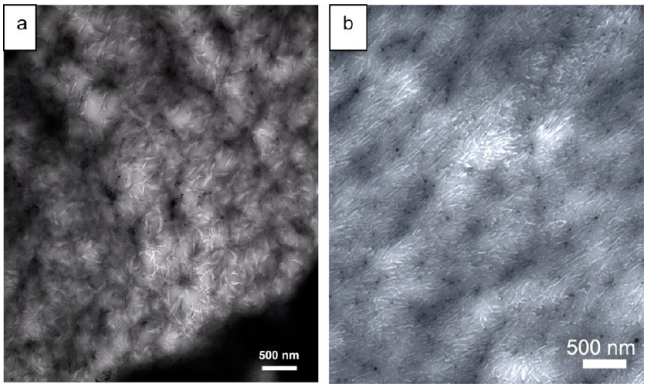

Figure 5. Transmission electron micrographs of nanocomposites obtained via (a) solution casting approach (**c**-series), loaded with 17% v/v of CNCs, and (b) template approach (**t**-series), loaded with 14% v/v of CNCs showing rod-shaped CNCs dispersed in the SBR matrix (low contrast). Images were taken after cryo-microtoming at −70 °C.

equilibrium degree of swelling steadily increases from 6% for neat SBR (**0t**) to 19% for the nanocomposite with 22% v/v CNCs (**22t**). Thus, in spite of the hydrophobicity of the neat SBR, water can be taken up by these nanocomposites. A similar behavior was observed before when SBR was reinforced with CNCs isolated from tunicates.[22] This phenomenon is ascribed to the hydrophilic nature of the CNCs that promotes the diffusion of water within the hydrophobic SBR matrix. The diffusion coefficient, D, of water in the CNC based nanocomposite films obtained by the template approach (**t**-series) can be estimated using eq 3. The plots of $(M_t - M_0)/M_\infty$ as a function of $(t)^{1/2}$ were performed for all samples and the diffusion coefficients D, calculated from the slope of the early segments of these plots. The results indicated that D dramatically increases with increasing CNC content, i.e, from 2.4×10^{-12} cm^2 s^{-1} for the hydrophobic SBR sample (**0t**) to 14.5×10^{-12}, 17.3×10^{-12}, 24.3×10^{-12}, 28.3×10^{-12}, and 48.4×10^{-12} cm^2 s^{-1} for template-made nanocomposites with 10, 14, 16, 18, and 22% v/v CNCs, respectively. This increase in the diffusion rate by a factor of 20 is consistent with the presence of a three-dimensional percolating cellulose network within SBR matrix that promotes water diffusion.

Water-Responsive Mechanical Behavior. The wet-state tensile storage moduli E' of these nanocomposites after equilibrium swelling in deionized water for 6 days at 37 °C (for solution-cast and compression-molded samples) and 10 days at 23−25 °C (for samples made by the template approach) were determined by DMTA using a submersion clamp where the swollen samples were submerged in deionized water during an isothermal run at room temperature under tensile loading for 15 min. Experimental data of the wet state moduli at room temperature for nanocomposite samples obtained via solution casting (**c**-series), compression-molding (**m**-series), and the template approach (**t**-series), respectively are shown in Figure 3a, b. and c. Gratifyingly, all of the water-swollen samples show a significant decrease in E' compared to the dry state. The data show that the extent of mechanical switching depends on the CNC content and the processing method. No water-induced switching was observed for the neat SBR processed by the template method (**0t**), consistent with the limited water absorption of this material and the absence of any plasticization upon swelling. A modulus reduction from 3 to 1.1 MPa and 2 to 0.7 MPa was observed for the SBR latex processed by solution casting (**0c**) and compression-molding (**0m**), respectively, as a result of the substantial water absorption of these samples. In all three series E' increases, as expected, with the CNC content. The largest contrast was observed for the solution cast samples, where E' decreased from 736 MPa (dry state at 25 °C) to 6 MPa (wet state at 37 °C) in the case of the nanocomposite containing 20% v/v CNCs (**20c**, Figure 3a). In the case of the compression-molded samples the contrast was somewhat smaller due to the lower stiffness of the dry state; here E' showed a decrease from 210 MPa (dry state at 25 °C) to 5 MPa (wet state at 37 °C) for the same composition (**20m**) (Figure 3b). In the case of the template-made samples the contrast was still smaller, again due to the lower stiffness of the dry state; here E' showed a decrease from 78 MPa (dry state at 25 °C) to 14 MPa (wet state at 25 °C) for a similar composition (**22t**) (Figure 3c).The absolute differences of the moduli in the soft, water-swollen state of the three series are much smaller than in the dry state, where the moduli of compositions with comparable CNC content vary by up to an order of magnitude. The fact that the fabrication process has a smaller influence on the *absolute* value of the stiffness of the water-swollen nanocomposites than in the dry state seems to be consistent with the interpretation that filler−filler interactions are present in the dry state (which appear to

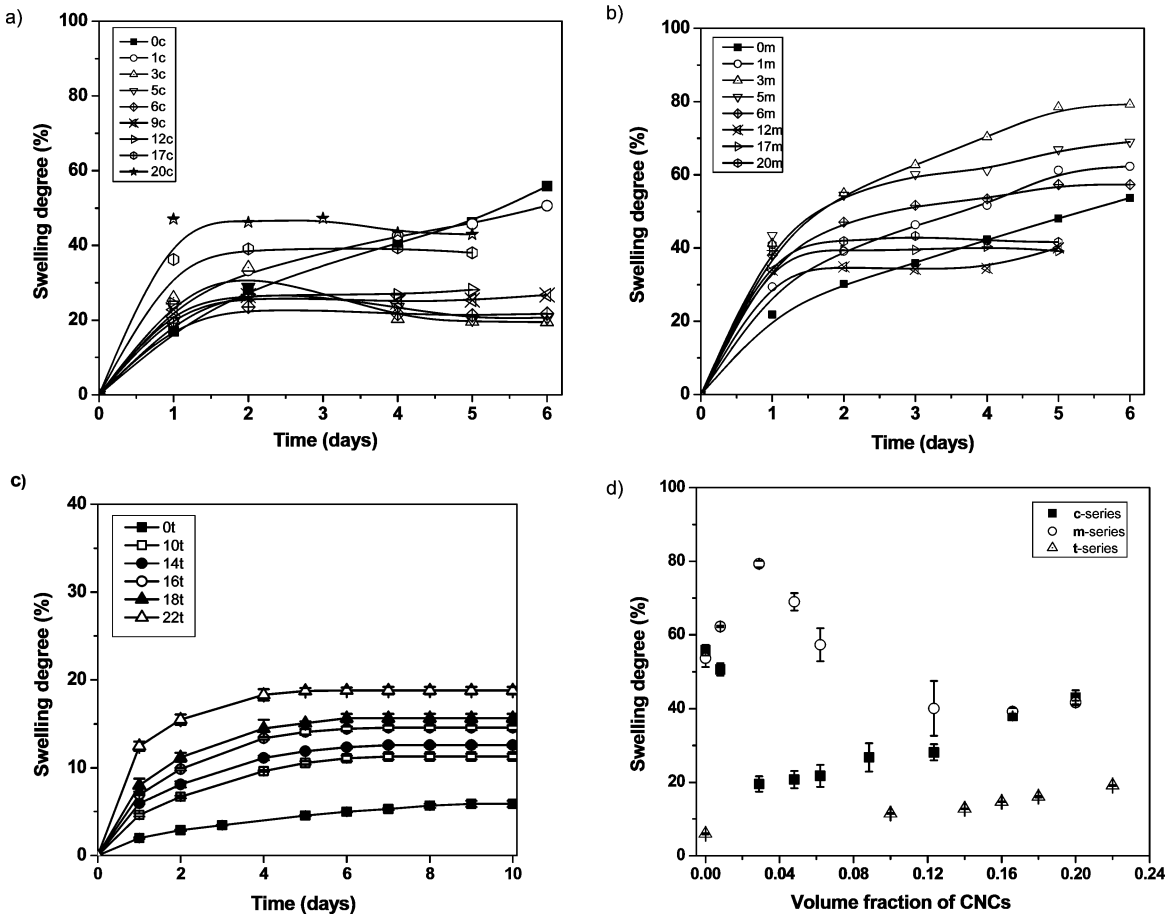

Figure 6. Swelling degree of SBR/CNC nanocomposites in deionized water as a function of CNC content and immersion time for (a) solution-cast (**c**-series) and (b) compression-molded (**m**-series) samples at 37 °C and (c) template-made (**t**-series) samples at room temperature. (d) Equilibrium swelling degree (for **c**- and **m**-series after 5−6 days and for **t**-series after 10 days) as a function of composition. Experimental data points represent averages (number of individual measurement, N = 3−4) ± standard error measurements.

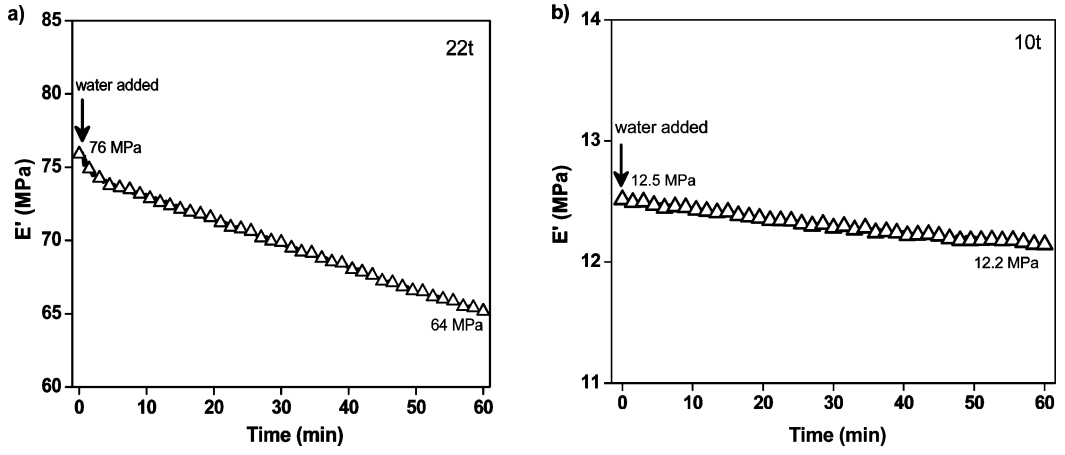

Figure 7. Representative data showing the change of E' of SBR/CNCs nanocomposite films made by the template approach (**t**-series) with (a) 22 and (b) 10% v/v CNCs, upon placing the samples in deionized water at 23−25 °C, showing the kinetics of modulus stimuli-responsive behavior.

depend on the specific morphology, which in turn depends on the processing method) and become—as intended—less relevant upon exposure to water. The fact that the properties do not strongly depend on the degree of aqueous swelling (the swelling of **20c** and **20m** is about twice that of **22t**), further suggests that the properties are governed by the CNCs and not the swelling of the matrix. The experimental E' values at 25 °C of water swollen samples were therefore compared with the prediction made by the Halpin−Kardos model.[39] This model has successfully been used to describe the modulus of nanocomposites in which the filler is homogeneously dispersed in a polymer matrix and does not display pronounced filler−filler interactions,[40,41] notably also the soft state of several other series of water-responsive mechanically adaptive nanocomposites studied by us before.[2,4,12,19] The details of the Halpin−Kardos model can be found in the Supporting Information. For

dx.doi.org/10.1021/am404382x | ACS Appl. Mater. Interfaces 2014, 6, 967−976

predicting E' of the water-swollen nanocomposites at 25 °C, the following parameters were used in connection with the Halpin–Kardos model: A = 10.5, E'_{lr} = 105 GPa,[13,42] E'_{tr} = 5 GPa, G_r = 1.77 GPa, ν_s = 0.3, and ν_r = 0.5.[43] The E'_s values of the water-swollen neat matrices at 25 °C used are 1.1, 0.7, and 1 MPa for casted, casted-compression-molded, and template-made samples, respectively.

A comparison of the experimental data (Figure 3a–c) and the predicted values shows that the moduli of all water-swollen SBR/CNC nanocomposite samples match the predicted values of the Halpin–Kardos model reasonably well, regardless of the processing technique. Thus, the mechanical contrast between the dry and wet states demonstrates that the presently investigated SBR/CNC nanocomposites do exhibit a stimuli-responsive mechanically dynamic behavior. The stimuli-responsive behavior was found to be completely reversible. Indeed, drying the nanocomposites restores their original mechanical stiffness as shown in Figure 3a–c (Representative plots of samples after redrying showing the evolution of E' as a function of temperature are displayed in Figure S2).

While the data in Figure 6 reveals that it can take up to several days for equilibrium water swelling in these nanocomposites (which is much slower than was shown for nanocomposites with more hydrophilic matrices, e.g. the poly(vinyl acetate)[4] or poly(vinyl alcohol)[14]), it is of interest to understand the initial rate of softening after placing the nanocomposites in water. Thus, the SBR/CNC nanocomposite samples obtained via the template approach (**t**-series) were mounted dry in a submersible clamp and their moduli were measured by DMTA in an isothermal run at 23–25 °C after adding deionized water. Representative plots displayed in Figure 7a and b show the change of E' upon placing the nanocomposites films in an aqueous environment of 22% v/v CNC and 10% v/v CNC, respectively.

As expected, it can be seen that the kinetics of modulus change depends strongly on the CNC content upon adding water. Over 60 min, a stimuli-responsive behavior, i.e. decrease in modulus, can be observed for 22, 18, and 16% v/v CNC samples; whereas for 10 and 14% v/v CNC samples this is less evident. The percentage decrease in E' that occurs within the first hour (relative to the wet modulus) is 16, 9, and 6% for 22, 18, and 16% v/v CNC samples, respectively.

To demonstrate the dynamics of the softening and stiffening of the nanocomposites upon immersion and drying, the mechanical properties were established using the above-mentioned setup that allowed the samples to be submerged in water throughout the tests. These results are of course strongly influenced by sample composition, dimension, and the drying conditions. Figure 8 shows the evolution of E' of the compression-molded SBR/CNC nanocomposite sample having 9% v/v CNCs (9m) as a function of time at a temperature of 37 °C, during wetting and drying.

An exponential decrease of E' can be observed after water addition, and within about 30 min (inset), the stiffness stabilized to the level of the wet state. As the switching process is related to diffusion of water in and out of the material, kinetics is related to the film thickness (~370 μm). After removal of water, E' increased steadily to regain the original stiffness, although this process was much slower than the wetting, lasting about 6–8 h. Repeated wetting and drying showed that the water induced modulus change is reversible and reproducible.

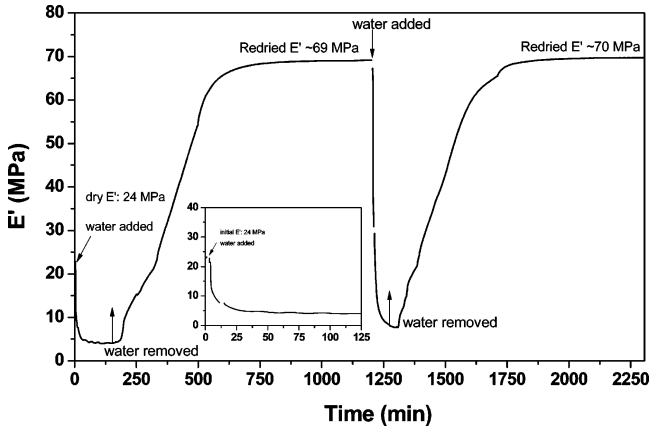

Figure 8. Storage modulus E' of compression-molded SBR/CNC nanocomposite films (**9m**) as a function of time at 37 °C, showing subsequent drying, wetting, and drying cycles within in the DMTA instruments. (inset) Decrease in E' (MPa) occuring within 2 h after the addition of water.

CONCLUSIONS

We studied the incorporation of hydrophilic cellulose nanocrystals into soft hydrophobic styrene butadiene rubber matrices to create water-responsive mechanically adaptive nanocomposites. The characterization revealed that the processing method has a significant influence on the morphology of the SBR nanocomposites, which in turn influences the stimuli-responsive mechanical properties of the materials, in particular the extent of mechanical reinforcement, the mechanical contrast, and the swelling behavior and kinetics of modulus switching. The findings are consistent with different arrangements of the CNCs, which serve as channels for water absorption and transport within the hydrophobic SBR matrix on the one hand and as switchable reinforcing filler on the other. In the case of the latex-based materials, the extent of aqueous swelling is significantly influenced by the surfactants present in the system. However, chemoresponsive behavior was established in all cases, despite the hydrophobic nature of the SBR matrix.

ASSOCIATED CONTENT

Supporting Information

Protocol for the isolation of CNCs and charge density measurements, details of the mechanical models used to predict the modulus of the SBR/CNC nanocomposites, and additional dynamic mechanical analyses data. This material is available free of charge via the Internet at http://pubs.acs.org.

AUTHOR INFORMATION

Corresponding Authors

*E-mail: christoph.weder@unifr.ch.
*E-mail: stuart.rowan@case.edu.

Present Address

[⊥]Australian Institute for Bioengineering and Nanotechnology, The University of Queensland, Brisbane 4072, Australia.

Author Contributions

[§]These authors contributed equally.

Notes

The authors declare no competing financial interest.

■ ACKNOWLEDGMENTS

The authors gratefully acknowledge financial support from the US National Science Foundation under Grant No. DMR-1204948, the Swiss National Science Foundation (NRP 62: Smart Materials, Nr. 406240_126046), the Kent H. Smith Charitable Trust (S.J.R.), and the Adolphe Merkle Foundation (C.W.). We also thank Mehdi Jorfi and Mahesh Biyani for technical assistance.

■ REFERENCES

(1) Roy, D.; Cambre, J. N.; Sumerlin, B. S. *Prog. Polym. Sci.* **2010**, *35*, 278−301.
(2) Capadona, J. R.; Shanmuganathan, K.; Tyler, D. J.; Rowan, S. J.; Weder, C. *Science* **2008**, *319*, 1370−1374.
(3) Shanmuganathan, K.; Capadona, J. R.; Rowan, S. J.; Weder, C. *Prog. Polym. Sci.* **2010**, *35*, 212−222.
(4) Shanmuganathan, K.; Capadona, J. R.; Rowan, S. J.; Weder, C. *ACS Appl. Mater. Interf.* **2010**, *2*, 165−174.
(5) Eichhorn, S. J.; Dufresne, A.; Aranguren, M.; Marcovich, N. E.; Capadona, J. R.; Rowan, S. J.; Weder, C.; Thielemans, W.; Roman, M.; Renneckar, S.; Gindl, W.; Veigel, S.; Keckes, J.; Yano, H.; Abe, K.; Nogi, M.; Nakagaito, A. N.; Mangalam, A.; Simonsen, J.; Benight, A. S.; Bismarck, A.; Berglund, L. A.; Peijs, T. *J. Mater. Sci.* **2010**, *45*, 1−33.
(6) Klemm, D.; Kramer, F.; Moritz, S.; Lindstrom, T.; Ankerfors, M.; Gray, D.; Dorris, A. *Angew. Chem., Int. Ed.* **2011**, *50*, 5438−5466.
(7) Clift, M. J. D.; Foster, E. J.; Vanhecke, D.; Studer, D.; Wick, P.; Gehr, P.; Rothen-Rutishauser, B.; Weder, C. *Biomacromolecules* **2011**, *12*, 3666−3673.
(8) Eichhorn, S. J. *ACS Macro Lett.* **2012**, *1*, 1237−1239.
(9) Rusli, R.; Shanmuganathan, K.; Rowan, S. J.; Weder, C.; Eichhorn, S. J. *Biomacromolecules* **2010**, *11*, 762−768.
(10) Rusli, R.; Shanmuganathan, K.; Rowan, S. J.; Weder, C.; Eichhorn, S. J. *Biomacromolecules* **2011**, *12*, 1363−1369.
(11) Fox, J. D.; Capadona, J. R.; Marasco, P. D.; Rowan, S. J. *J. Am. Chem. Soc.* **2013**, *135*, 5167−5174.
(12) Hsu, L.; Weder, C.; Rowan, S. J. *J. Mater. Chem.* **2011**, *21*, 2812−2822.
(13) Shanmuganathan, K.; Capadona, J. R.; Rowan, S. J.; Weder, C. *J. Mater. Chem.* **2010**, *20*, 180−186.
(14) Jorfi, M.; Roberts, M. N.; Foster, E. J.; Weder, C. *ACS Appl. Mater. Interf.* **2013**, *5*, 1517−1526.
(15) Hess, A. E.; Capadona, J. R.; Shanmuganathan, K.; Hsu, L.; Rowan, S. J.; Weder, C.; Tyler, D. J.; Zorman, C. A. *J. Micromech. Microeng.* **2011**, *21*, 054009.
(16) Harris, J. P.; Hess, A. E.; Rowan, S. J.; Weder, C.; Zorman, C. A.; Tyler, D. J.; Capadona, J. R. *J. Neural. Eng.* **2011**, *8*, 046010.
(17) Harris, J. P.; Capadona, J. R.; Miller, R. H.; Healy, B. C.; Shanmuganathan, K.; Rowan, S. J.; Weder, C.; Tyler, D. J. *J. Neural. Eng.* **2011**, *8*, 066011.
(18) Capadona, J. R.; Tyler, D. J.; Zorman, C. A.; Rowan, S. J.; Weder, C. *MRS Bull.* **2012**, *37*, 581−589.
(19) Mendez, J.; Annamalai, P. K.; Eichhorn, S. J.; Rusli, R.; Rowan, S. J.; Foster, E. J.; Weder, C. *Macromolecules* **2011**, *44*, 6827−6835.
(20) Way, A. E.; Hsu, L.; Shanmuganathan, K.; Weder, C.; Rowan, S. J. *ACS Macro Lett.* **2012**, *1*, 1001−1006.
(21) Biyani, M. V.; Foster, E. J.; Weder, C. *ACS Macro Lett.* **2013**, *2*, 236−240.
(22) Dagnon, K. L.; Shanmuganathan, K.; Weder, C.; Rowan, S. J. *Macromolecules* **2012**, *45*, 4707−4715.
(23) Capadona, J. R.; Van Den Berg, O.; Capadona, L. A.; Schroeter, M.; Rowan, S. J.; Tyler, D. J.; Weder, C. *Nat. Nanotechnol.* **2007**, *2*, 765−769.
(24) Ben Azouz, K.; Ramires, E. C.; Van den Fonteyne, W.; El Kissi, N.; Dufresne, A. *ACS Macro Lett.* **2012**, *1*, 236−240.
(25) Ma, H. Y.; Burger, C.; Hsiao, B. S.; Chu, B. *ACS Macro Lett.* **2012**, *1*, 723−726.
(26) Favier, V.; Chanzy, H.; Cavaille, J. Y. *Macromolecules* **1995**, *28*, 6365−6367.
(27) Dong, X. M.; Kimura, T.; Revol, J. F.; Gray, D. G. *Langmuir* **1996**, *12*, 2076−2082.
(28) Espinosa, S. C.; Kuhnt, T.; Foster, E. J.; Weder, C. *Biomacromolecules* **2013**, *14*, 1223−1230.
(29) Sun, C. C. *Int. J. Pharm.* **2008**, *346*, 93−101.
(30) Tang, L. M.; Weder, C. *ACS Appl. Mater. Interf.* **2010**, *2*, 1073−1080.
(31) Capadona, J. R.; Shanmuganathan, K.; Trittschuh, S.; Seidel, S.; Rowan, S. J.; Weder, C. *Biomacromolecules* **2009**, *10*, 712−716.
(32) Angles, M. N.; Dufresne, A. *Macromolecules* **2000**, *33*, 8344−8353.
(33) Dagnon, K. L.; Way, A. E.; Carson, S. O.; Silva, J.; Maia, J.; Rowan, S. J. *Macromolecules* **2013**, *46*, 8203−8212.
(34) Wang, N.; Ding, E. Y.; Cheng, R. S. *Polymer* **2007**, *48*, 3486−3493.
(35) Kumar, S.; Hofmann, M.; Steinmann, B.; Foster, E. J.; Weder, C. *ACS Appl. Mater. Interf.* **2012**, *4*, 5399−5407.
(36) Dubief, D.; Samain, E.; Dufresne, A. *Macromolecules* **1999**, *32*, 5765−5771.
(37) Amalvy, J. I.; Unzue, M. J.; Schoonbrood, A. S.; Asua, J. M. *J. Polym. Sci., Polym. Chem.* **2002**, *40*, 2994−3000.
(38) Kawamukai, T.; Ishii, E.; Yagi, H. *Tappi J.* **2001**, *84*, 51−51.
(39) Halpin, J. C.; Kardos, J. L. *J. Appl. Phys.* **1972**, *43*, 2235−2241.
(40) Helbert, W.; Cavaille, J. Y.; Dufresne, A. *Polym. Composite* **1996**, *17*, 604−611.
(41) Favier, V.; Canova, G. R.; Cavaille, J. Y.; Chanzy, H.; Dufresne, A.; Gauthier, C. *Polym. Adv. Technol.* **1995**, *6*, 351−355.
(42) Rusli, R.; Eichhorn, S. J. *Appl. Phys. Lett.* **2008**, *93*, 033111.
(43) Hajji, P.; Cavaille, J. Y.; Favier, V.; Gauthier, C.; Vigier, G. *Polym. Composite* **1996**, *17*, 612−619.